

Observation of fast collinear partitioning of the $^{197}\text{Au} + ^{197}\text{Au}$ system into three and four fragments of comparable size

J. Wilczyński,^{1,*} I. Skwira-Chalot,² K. Siwek-Wilczyńska,² A. Pagano,³ F. Amorini,^{4,5} A. Anzalone,^{4,5} L. Auditore,⁶ V. Baran,^{4,7} J. Brzychczyk,⁸ G. Cardella,³ S. Cavallaro,^{4,5} M. B. Chatterjee,⁹ M. Colonna,^{4,5} E. De Filippo,³ M. Di Toro,^{4,5} W. Gawlikowicz,¹⁰ E. Geraci,^{3,5} A. Grzeszczuk,¹¹ P. Guazzoni,¹² S. Kowalski,¹¹ E. La Guidara,³ G. Lanzalone,^{4,13} J. Łukasik,¹⁴ C. Maiolino,^{4,5} Z. Majka,⁸ N. G. Nicolis,¹⁵ M. Papa,³ E. Piasecki,^{1,10} S. Pirrone,³ R. Płaneta,⁸ G. Politi,^{3,5} F. Porto,^{4,5} F. Rizzo,^{4,5} P. Russotto,^{4,5} K. Schmidt,¹¹ A. Sochocka,⁸ Ł. Świdorski,¹ A. Trifirò,⁶ M. Trimarchi,⁶ J. P. Wieleczko,¹⁶ L. Zetta,¹² and W. Zipper¹¹

¹*The Andrzej Sołtan Institute for Nuclear Studies, Świerk/Warsaw, Poland*

²*Institute of Experimental Physics, University of Warsaw, Warsaw, Poland*

³*INFN, Sezione di Catania, Catania, Italy*

⁴*INFN, Laboratori Nazionali del Sud, Catania, Italy*

⁵*Dipartimento di Fisica e Astronomia, Università di Catania, Catania, Italy*

⁶*INFN, Gruppo Collegato di Messina and Dipartimento di Fisica, Università di Messina, Messina, Italy*

⁷*University of Bucharest and NIPNE-HH, Bucharest, Romania*

⁸*The Marian Smoluchowski Institute of Physics, Jagiellonian University, Cracow, Poland*

⁹*Saha Institute of Nuclear Physics, Kolkata, India*

¹⁰*Heavy Ion Laboratory, University of Warsaw, Warsaw, Poland*

¹¹*Institute of Physics, University of Silesia, Katowice, Poland*

¹²*INFN, Sezione di Milano and Dipartimento di Fisica, Università di Milano, Milano, Italy*

¹³*Università degli Studi di Enna "Kore," Enna, Italy*

¹⁴*The Henryk Niewodniczański Institute of Nuclear Physics, Cracow, Poland*

¹⁵*Department of Physics, University of Ioannina, Ioannina, Greece*

¹⁶*GANIL, CEA, IN2P3-CNRS, Caen, France*

(Received 11 November 2009; published 12 February 2010)

Collisions of a very heavy nonfusing nuclear system $^{197}\text{Au} + ^{197}\text{Au}$ were studied at an energy of 15 MeV/nucleon. An interesting process of violent reseparation of this heavy system into three or four fragments of comparable size was observed. In the case of ternary partitioning, either the projectile-like fragment (PLF) or target-like fragment (TLF) breaks up almost collinearly with the PLF-TLF separation axis. In the case of quaternary reactions, both PLF and TLF were observed breaking up along this direction. By comparison with a dynamical model of deep inelastic collisions it was concluded that the ternary and quaternary reactions occur in semiperipheral collisions, in a range of angular momenta corresponding to about 0.5–0.7 of the maximum L value for grazing collisions. The time elapsing from the scission of the binary PLF + TLF system to the secondary scission of PLF or TLF was estimated to be of about 70–80 fm/c for the ternary reactions and 80–100 fm/c for the quaternary reactions.

DOI: [10.1103/PhysRevC.81.024605](https://doi.org/10.1103/PhysRevC.81.024605)

PACS number(s): 25.70.Lm, 25.70.Mn

I. INTRODUCTION

Our current understanding of the dynamics of nucleus-nucleus collisions at energies below 20 MeV/nucleon is limited mostly to peripheral reactions because the central and semiperipheral collisions of typical systems studied so far led, in general, to the fusion and formation of the compound nucleus. The usually observed nonfusion processes were found to be basically binary deep-inelastic reactions, called also dissipative or strongly damped collisions (see, e.g., review article by Gobbi and Nörenberg [1]). The characteristic features of these deep-inelastic reactions are the continuous loss of relative kinetic energy and the broadening of the mass distribution of the interacting fragments with the increasing loss of kinetic

energy—both effects due to the intense exchange of nucleons during the collision.

For typical combinations of the projectile and target nuclei, the interacting composite system either reseparates (in peripheral collisions) or fuses and forms a compound nucleus (for central and semiperipheral collisions). New, experimentally unexplored processes, may occur in collisions of very heavy and rather symmetric systems that, due to strong Coulomb repulsion, cannot fuse at all, even in central collisions. Consequently, the colliding nuclei must reseparate avoiding the intermediate stage of the compound nucleus. An open question is what kind of partitioning of the interacting system can be observed in these close collisions of very heavy systems. One can find in the literature both experimental and theoretical indications that reactions involving heavy, mostly symmetric systems may reveal interesting new phenomena in their reseparation and partition.

* Corresponding author: wilczynski@ipj.gov.pl

For example, calculations in terms of the Los Alamos finite-range macroscopic dynamical model [2] suggested that dynamical evolution in the multidimensional deformation space may lead to multifragment scission configurations (with one or two massive fragments formed in the neck region), mostly for very heavy composite systems of A of the order of 300–400, especially when the two-body dissipation mechanism is assumed.

The ternary partitioning processes were already observed in early experiments [3,4] employing mica detectors in which three fragments of nearly equal size were observed in Ar and Fe-induced reactions on heavy targets at energies of about 10 MeV/nucleon. However, the detection technique did not allow one to determine whether the fragments result from sequential statistical fission of the heavy nucleus following a conventional dissipative collision in the primary stage of the reaction or if they were produced in a dynamical process.

In later experiments reported by Glässel *et al.* [5] and Stefanini *et al.* [6] the dynamical character of the ternary breakup was demonstrated for a part of the ternary events. A clear effect of nonequilibrium fission of primary projectile-like fragments from the $^{129}\text{Xe} + ^{122}\text{Sn}$ reaction at 12.5 MeV/nucleon was reported by Glässel *et al.* [5]. In a more recent work, Stefanini *et al.* [6] observed similar effects in $^{100}\text{Mo} + ^{100}\text{Mo}$ and $^{120}\text{Sn} + ^{120}\text{Sn}$ collisions at about 20 MeV/nucleon. In both these studies [5,6] the dynamical partitioning processes coexisted with the background of the equilibrium (statistical) fission of one of the reaction partners. Quaternary partitioning of heavy colliding systems was also reported in the past [7], but the nature of these reactions (statistical or dynamical) was not investigated.

In our recent article [8] we demonstrated the presence of the mechanism of fast ternary and quaternary breakup of a very heavy nuclear system $^{197}\text{Au} + ^{197}\text{Au}$ in collisions at 15 MeV/nucleon. It was shown that, in sufficiently inelastic collisions, the colliding system gets torn apart into three or four massive fragments, which in the dominant part of events are nearly aligned along a common reseparation axis.

It is important to note that the reactions of ternary and quaternary breakup into fragments of comparable size, observed in collisions of very heavy systems at energies below 20 MeV/nucleon, should not be mixed up with the very asymmetric projectile partitioning observed at the Fermi-energy domain (see Refs. [9,10]), interpreted as neck fragmentation processes and well described by the stochastic Boltzmann-Nordheim-Vlasov (BNV) [11] and the Constrained Molecular Dynamics II (CoMD-II) [12] models. In the latter processes, relatively small fragments (intermediate mass fragments, IMF) are emitted from the neck region, while in the former reactions the observed fragments seem to originate largely from the nearly symmetric nonequilibrium breakup of the primary products of deep-inelastic reactions.

In the present article we give a detailed account of a study signalized in our Letter [8]. We demonstrate the presence of the mechanism of dynamical (aligned) ternary and quaternary breakup of a very heavy nuclear system $^{197}\text{Au} + ^{197}\text{Au}$ into fragments of comparable size, in collisions at 15 MeV/nucleon. The mass and angular distributions of fragments in these processes are presented. Attempts to deduce

the time scale of these exotic breakup processes and also their localization in the angular momentum space will be presented.

II. EXPERIMENT

The experiment was carried out at the Laboratori Nazionali del Sud (LNS) in Catania, Italy. A beam of ^{197}Au ions from the LNS Superconducting Cyclotron was accelerated to the energy of 2900 MeV and bombarded a $273 \mu\text{g}/\text{cm}^2$ -thick ^{197}Au target placed inside the Charged Heavy Ion Mass and Energy Resolving Array (CHIMERA). The CHIMERA multidetector, arranged in 4π geometry, is built of 1192 two-layer ΔE - E telescopes, each telescope consisting of a planar $300 \mu\text{m}$ -silicon detector and a CsI(Tl) scintillator. For more details concerning the CHIMERA multidetector see Refs. [13,14].

Most fragments originating from the $^{197}\text{Au} + ^{197}\text{Au}$ collisions were stopped in the silicon detectors. Mass determination of these fragments was achieved by combining energy and time-of-flight (TOF) measurements. The energy resolution of most of the silicon detectors for fully stopped ^{197}Au ions (2900 MeV) was about 1%.

The TOF measurements were done using the timing signal from the silicon detectors relative to the timing of the cyclotron high frequency signal. An overall time resolution of $\delta t \approx 0.8$ – 1.2 ns (full width at half maximum, FWHM) was achieved. This resulted in the mass resolution in a range from 3% at forward angles up to about 8% in the worst case when TOF was measured on a relatively short distance of 40 cm in detectors of the “sphere” part of CHIMERA [13,14]. This rather poor mass resolution, mostly affecting target-like fragments at large angles is not, however, critical regarding the main goals of the experiment.

The fact that the detection of fragments was based exclusively on the energy and TOF measurements in the CHIMERA front-layer silicon detectors had the virtue of negligibly low energy thresholds in the data. The information on light charged particles requiring signals from the CsI(Tl) detectors was not used in the present analysis.

Energy calibration of the silicon detectors was done using elastic scattering of ^{197}Au ions from the LNS cyclotron as well as elastic scattering of ^{12}C and ^{16}O beams from the MP Tandem accelerator in additional calibration runs at different energies. Fission fragments from the $^{12}\text{C} + ^{197}\text{Au} \rightarrow ^{209}\text{At}$ reaction of a known average kinetic energy [15] were also used to check the calibration of midmass fragments and to control the stability of measurements throughout the experiment. Energies of target-like fragments in detectors within the angular range $70^\circ \leq \theta_{\text{lab}} \leq 86^\circ$ were calibrated using a technique based on the in-plane Au + Au inelastic scattering coincidences.

The TOF calibration was done for Au ions in a very wide dynamical range and also for fission fragments from the $^{12}\text{C} + ^{197}\text{Au} \rightarrow ^{209}\text{At}$ reaction, as well as for several light ions (Li, Be) identified in the energy versus time spectra, stopped in the silicon detectors. The TOF offset parameter t_0 in the relation between the kinetic energy and TOF was then determined as a function of energy and mass for a given group of fragments, individually in each detector. Effective values of t_0 for other fragments were obtained by interpolation.

III. SELECTION OF EVENTS FOR ANALYSIS

In the analysis of Au + Au collisions we concentrated on approximately complete events in which few massive fragments are formed after the collision. All light particles accompanying the fragments, mostly neutrons, protons, and α particles, were assumed to be evaporated from the excited fragments. Individual information on these light particles was discarded. Thus the selected data contained complete information only on charged fragments of $Z \geq 3$ in a given event, while light particles presumably originating from evaporation processes were accounted for only in the balance of mass and momentum. (It was assumed throughout the whole analysis that the evaporated light particles do not influence *velocities* of the fragments.)

Events containing information on all fragments of $Z \geq 3$ recorded by any detector of the CHIMERA array within the angular range $2.6^\circ \leq \theta_{\text{lab}} \leq 86^\circ$ represented the basic set of the collected data. The smallest detection angles (close to the beam direction, $\theta_{\text{lab}} < 2.6^\circ$) were excluded in this experiment to prevent these most forward detectors from the very intensive rate of elastically scattered Au ions. Due to the large center-of-mass velocity in collisions of the symmetric Au + Au system, the limitation of the laboratory detection angles to $\theta_{\text{lab}} < 86^\circ$ was sufficient in detecting almost all heavy fragments of interest. (The angular range $86^\circ \leq \theta_{\text{lab}} \leq 94^\circ$ was inaccessible anyway due to the shadowing detectors by the target being placed perpendicularly to the beam.)

A survey of the events selected with the condition $Z \geq 3$ showed that the collected data contain predominantly binary, ternary, and quaternary events with a practically negligible contribution of higher multiplicities of fragments (see Fig. 1). With a trigger rejecting elastic and quasielastic scattering, the binary events (about 84% of the collected data) are dominated by deep-inelastic reactions showing excitation energies up to 200–300 MeV. The remaining part of the collected data represent reactions with three and four large fragments in the final state (13% and 3% of the total number of the recorded events, respectively) which, on average, are characterized by even higher excitation energies and show features of a new, very fast reaction mechanism.

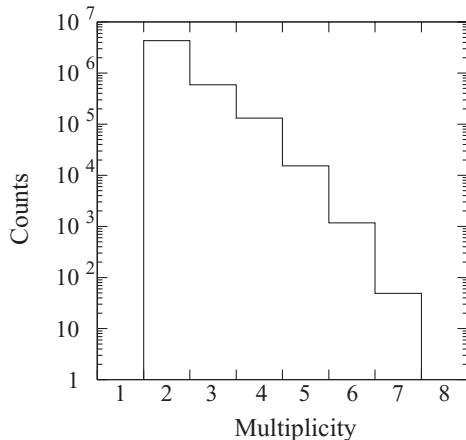


FIG. 1. Multiplicity distribution of fragments of $Z \geq 3$ in the $^{197}\text{Au} + ^{197}\text{Au}$ reaction at 15 MeV/nucleon.

IV. TERNARY REACTIONS

Ternary events were selected under the condition of nearly complete balance of mass, allowing, however, for up to 70 mass units to be lost due to the evaporation of undetected nucleons and α particles from the excited primary fragments

$$A_{\text{projectile}} + A_{\text{target}} - 70 \leq A_1 + A_2 + A_3 \leq A_{\text{projectile}} + A_{\text{target}}, \quad (1)$$

where A_1 , A_2 , and A_3 are the mass numbers of three detected fragments and $A_{\text{projectile}} = A_{\text{target}} = 197$. This limit of 70 mass units in evaporated light particles covered the essential part of the dynamical range of the observed reactions and was based on shapes of the summed mass and kinetic energy spectra of all three fragments in the ternary events.

To reject incomplete or incorrectly reconstructed events, conditions on the balance of longitudinal and transversal momenta were imposed

$$\left| \sum_{i=1}^3 \vec{p}_{\text{long}}(i) \right| > 0.8 p_0, \quad (2)$$

$$\left| \sum_{i=1}^3 \vec{p}_{\text{trans}}(i) \right| < 0.04 p_0, \quad (3)$$

where p_0 is the momentum of ^{197}Au projectiles. The earlier lower limit for the longitudinal momentum is consistent with the loss of mass allowed for evaporation.

It is interesting to examine correlations between mass numbers of fragments in the selected ternary events that satisfy Eqs. (1) through (3). In a triangular Dalitz-type diagram (see Fig. 2) each ternary event with fragments of mass numbers A_1 , A_2 , and A_3 is represented by a point placed at distances from three sides of the equilateral triangle by A_1/A , A_2/A , and A_3/A , respectively, where $A = A_1 + A_2 + A_3$. The events are concentrated mostly in three regions characterized by the presence of one heavy fragment approximately within a range of mass numbers $0.38 < A_i/A < 0.53$ and two lighter (comparable in mass) fragments approximately within $0.15 < A_i/A < 0.38$. (Three intensely populated regions in Fig. 2 reflect three permutations of A_1 , A_2 , and A_3 in the same event.)

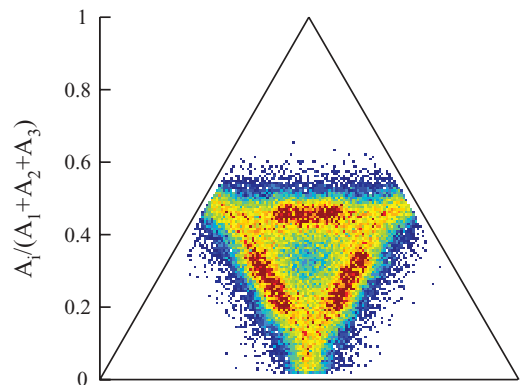


FIG. 2. (Color online) Dalitz diagram representing nearly complete events of ternary partitioning of the $^{197}\text{Au} + ^{197}\text{Au}$ system. See text.

As the mass number of the heaviest fragment (within the range $0.38 < A_i/A < 0.53$) is close to the mass number of ^{197}Au , one can presume that the observed ternary events are dominated by processes in which the *heaviest* fragment is the remnant of the projectile [the projectile-like fragment (PLF)] or target [the target-like fragment (TLF)], while the two lighter fragments originate from the breakup of the complementary primary fragment (TLF or PLF, respectively). In other words, we assume that the observed ternary reactions proceed either as



or



From the point of view of the experiment, it is much easier to detect and identify all three fragments when TLF *survives* and PLF splits up. Therefore, only those events originating from the process (4) (representing exactly half of all ternary events in the symmetric Au + Au reaction) were analyzed. By choosing the projectile breakup (4) one requires that the heaviest fragment (TLF) is the *slowest* one. Consequently, the events were arranged according to the longitudinal velocities (in the laboratory system) by assigning

$$V_{\text{long}}(\text{F1}) > V_{\text{long}}(\text{F2}) > V_{\text{long}}(\text{TLF}), \quad (6)$$

while the previously mentioned limits of mass numbers (corresponding to the most intense group of events in the Dalitz plot) were imposed

$$150 \leq A_{\text{TLF}} \leq 210, \quad (7)$$

$$60 \leq A_{\text{F1}} < 150, \quad (8)$$

$$60 \leq A_{\text{F2}} < 150. \quad (9)$$

Reaction scheme (4) suggests a definite two-step reaction with a binary step, $^{197}\text{Au} + ^{197}\text{Au} \rightarrow \text{TLF} + \text{PLF}$, in the first stage of the reaction. In the following, we give arguments that make this assumption very plausible.

A strong argument in support of scheme (4) comes from examining the correlation between the relative velocity of the F1 + F2 subsystem and the kinetic energy of the relative motion of the total PLF + TLF system, $E_{\text{kin}}(\text{PLF} + \text{TLF})$. This correlation is shown in Fig. 3. To calculate $E_{\text{kin}}(\text{PLF} + \text{TLF})$, the velocity of PLF was reconstructed, event by event, as the velocity of the center of mass of the F1 + F2 subsystem. The relative velocity of fragments F1 and F2 is expressed in units of the “Viola velocity” $(V_{\text{rel}}/V_{\text{Viola}})_{\text{F1,F2}}$. Here, the Viola velocity V_{Viola} corresponds to the kinetic energy released in fission: For symmetric fission it is given by the systematics of Ref. [15] and for asymmetric fission a modified formula [16] is used. It is seen from Fig. 3 that the relative motion in the F1 + F2 subsystem is almost completely relaxed (i.e., these two fragments move with the kinetic energy not exceeding by much the energy of their mutual Coulomb repulsion). However, the relative motion in the PLF + TLF system is only partly damped. [According to the Viola systematics, the kinetic energy of the Coulomb repulsion for the $^{197}\text{Au} + ^{197}\text{Au}$ system is $E_{\text{Viola}}(^{197}\text{Au} + ^{197}\text{Au}) = 412 \text{ MeV}$.] This fact definitely suggests that the PLF + TLF system reseparates in the first

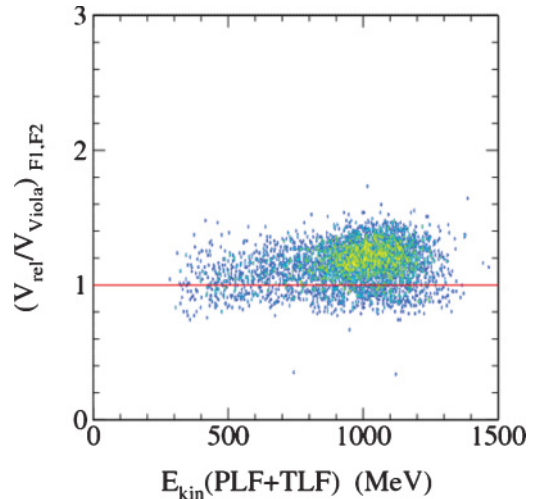


FIG. 3. (Color online) Relative velocity of the two fastest fragments F1 and F2 expressed in units of the “Viola velocity” $(V_{\text{rel}}/V_{\text{Viola}})_{\text{F1,F2}}$, plotted as a function of the kinetic energy of the relative motion of the total PLF + TLF system, $E_{\text{kin}}(\text{PLF} + \text{TLF})$.

stage of the reaction (with only partial damping of the kinetic energy of relative motion) and only then, in the next stage of the collision, does PLF breakup.

Another argument in support of the sequential scheme (4) comes from an analysis of mass distributions of fragments F1, F2, and TLF. All these distributions are shown in Fig. 4. Note that by definition the fragment F1 is faster (in the laboratory system) than F2 [see Eq. (6)]. Figure 4 shows also the reconstructed mass spectrum of PLF obtained by summing, event by event, the mass numbers of fragments F1 and F2: $A(\text{PLF}) = A(\text{F1}) + A(\text{F2})$. Clearly, the mass spectra

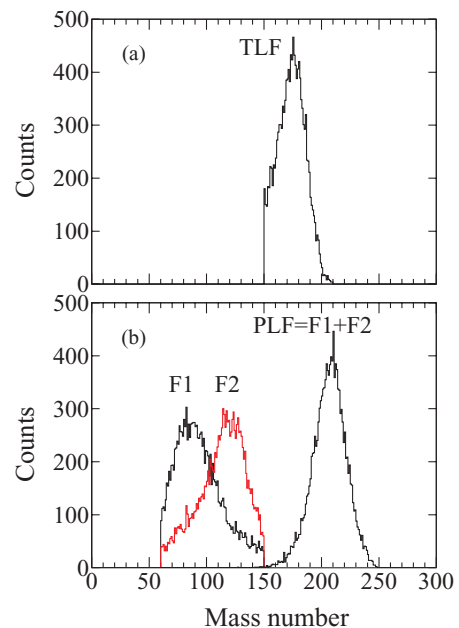


FIG. 4. (Color online) (b) Reconstructed mass spectrum of PLF's obtained by the event-by-event addition of mass numbers of fragments F1 and F2, compared with (a) the mass spectrum of TLF's.

of fragments F1 and F2 differ significantly, a fact that rather excludes purely statistical fission of PLF. On average, a lighter fragment moves in front of the heavier one, but the asymmetry of the partitioning of PLF is not large. We emphasize the fact that wide mass distributions of F1 and F2 sum up to a much narrower mass distribution of the reconstructed PLF. This fact is consistent with the assumption that fragments F1 and F2 originate from splitting PLF after the PLF gets separated from the TLF.

It is also interesting to note the asymmetry of the average mass numbers of TLF and PLF, despite the symmetry of the colliding $^{197}\text{Au} + ^{197}\text{Au}$ system. The larger masses of PLF (as compared with TLF) demonstrate that, in all likelihood, just the net transfer of mass between PLF and TLF triggers the splitting of one of the interacting nuclei, preferentially the acceptor nucleus that received more excitation energy and intrinsic spin due to the net transfer of nucleons. This phenomenon was known for a long time [17,18] in reactions at energies of about 10 MeV/nucleon. (Note also that the fissility of the acceptor nucleus is larger than the fissility of the donor nucleus.)

Prior to a detailed analysis of the selected ternary events we present in Fig. 5(a) an overview of these events in the form of a scatterplot where velocities of all three fragments are displayed in the transversal versus longitudinal velocity space. A subclass of nearly coplanar ($\pm 20^\circ$) events was selected for this display. (For the definition of the reaction plane and display of the out-of-plane distribution, see the next section.) In this plot, the sign of the transversal velocity in the reaction plane is distinguished by setting by definition the negative sign to the TLF (and automatically positive for the PLF). In such a way, all nearly coplanar ternary events are jointly visualized in a common reaction plane. It is seen from Fig. 5(a) that TLF is scattered at large angles ($V_{\text{long}} \approx 0.5$ cm/ns, $V_{\text{trans}} \approx -1.1$ cm/ns), while F1 and F2 are predominantly emitted at well-defined locations in the velocity space $V_{\text{long}} \approx 6.3$ cm/ns, $V_{\text{trans}} \approx 1.2$ cm/ns and $V_{\text{long}} \approx 3.4$ cm/ns, $V_{\text{trans}} \approx 0.7$ cm/ns, respectively. The most probable location of fragments F1 and F2 shows that the PLF breakup is sharply focused in one direction, nearly along the separation axis of TLF and PLF indicated in Figs. 5(a) and 5(b) by dashed lines. The approximate alignment of all three fragments along the TLF-PLF separation axis proves that the breakup of PLF is a violent process taking place in a very short time immediately after the separation of PLF from TLF. An attempt of a quantitative estimation of the time scale of this process is given in the next section.

In Fig. 5(b) we present a theoretical simulation of the ternary breakup of the $^{197}\text{Au} + ^{197}\text{Au}$ system in terms of the quantum molecular dynamics (QMD) model version of Łukasik [19]. The QMD ternary events were selected from a complete set of theoretical events generated within the entire range of impact parameters, with the same gates on fragments' mass numbers [Eqs. (7) through (9)] and for the same range of the out-of-plane angles of the PLF breakup ($\pm 20^\circ$) as in the experiment. The theoretical events in Fig. 5(b) are shown after filtering them through the detection filter [20] of the CHIMERA multidetector. It is seen from Fig. 5(b) that the QMD model correctly reproduces the inelasticity of the reaction because both TLF and the primary PLF are properly

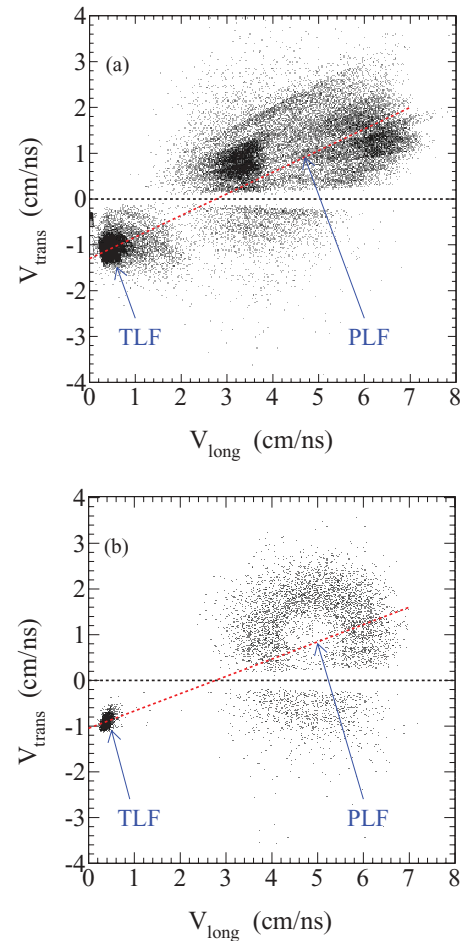


FIG. 5. (Color online) (a) In-plane velocity distribution of fragments from ternary partitioning of the $^{197}\text{Au} + ^{197}\text{Au}$ system in the experiment and (b) generated with the QMD code [19] (filtered with the CHIMERA detector filter). Points represent velocities of fragments F1, F2, and TLF in each event, plotted in the laboratory reference frame as a function of the longitudinal and transversal components. Positions of TLF and primary PLF are indicated by arrows. The dashed lines show the TLF-PLF separation axis. See text.

located in the velocity space. Moreover, the model predicts the phenomenon of the *dynamical* breakup of PLF into two fragments of comparable masses, but fails to reproduce the characteristic collinear emission observed in the experiment. Quite obviously, the PLF breakup happens in the experiment much faster than is predicted by the QMD model.

The QMD calculations were carried out for a standard set of parameters [21] determined in a survey of a broad range of intermediate energies. Particularly, the soft equation of state $K = 200$ MeV and a standard blocking of nucleon-nucleon collisions (with a factor 0.93) were assumed. The dynamical evolution of the colliding system was followed over the time of 3000 fm/c. After that time a procedure of the statistical-decay “cooling” by using the code GEMINI [22] with a multiparticle Coulomb trajectories routine [23] was applied to determine the final mass numbers and asymptotic deflection angles of the fragments. Most of the simulated $\text{PLF} \rightarrow \text{F1} + \text{F2}$ breakup events occurred within the 3000 fm/c span of the

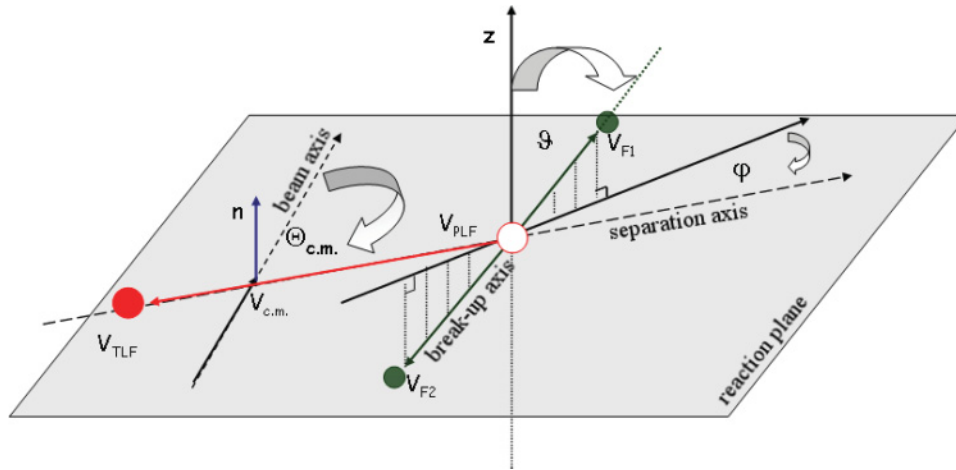


FIG. 6. (Color online) Scheme of the ternary decay process $^{197}\text{Au} + ^{197}\text{Au} \rightarrow \text{TLF} + \text{PLF} \rightarrow \text{TLF} + \text{F1} + \text{F2}$ that visualizes the velocity vectors and angles discussed in the text.

dynamical calculation and practically no F1 and F2 fragments can be attributed to the later stage described by the GEMINI code.

V. DETAILED ANALYSIS OF TERNARY EVENTS

Kinematical reconstruction of the studied events and their quantitative analysis require to define kinematical quantities in a convenient reference frame. The basic information on each ternary event originates from velocity vectors of fragments F1, F2, and TLF in the laboratory reference frame, $\vec{V}_{F1}(\text{laboratory})$, $\vec{V}_{F2}(\text{laboratory})$, and $\vec{V}_{TLF}(\text{laboratory})$ and masses M_{F1} , M_{F2} , and M_{TLF} , respectively, obtained from the measurements of the TOF and kinetic energy of these fragments.

Assuming that fragments F1 and F2 originate from the decay of PLF, one can reconstruct the asymptotic PLF velocity vector $\vec{V}_{PLF}(\text{laboratory})$ as the velocity of the center of mass of the F1 + F2 subsystem. It is then convenient to express quantities describing the relative motion of the binary TLF + PLF system in the reference frame of the center of mass of the total system, while the relative motion of the F1 + F2 subsystem in the rest frame of the PLF. In this approach, the scheme of the ternary decay process is shown in Fig. 6. In many respects it adopts a convention proposed in Ref. [6]. Thus the breakup of the colliding system into PLF and TLF occurs along the binary separation axis in the direction of the $\vec{V}_{PLF} - \vec{V}_{TLF}$ vector at an angle $\theta_{c.m.}$ with respect to the beam direction. The normal to the reaction plane \vec{n} is determined by the cross product of $\vec{V}_{PLF} - \vec{V}_{TLF}$ and the beam velocity vector.

The breakup of PLF occurs in the direction of the vector $\vec{V}_{F1} - \vec{V}_{F2}$, which is not restricted to the reaction plane. It is convenient to define the PLF breakup axis in polar coordinates in the PLF rest frame with the z axis parallel to \vec{n} (i.e., normal to the reaction plane). In this reference frame, the polar angle ϑ is measured between the z axis and the PLF breakup axis ($\vec{V}_{F1} - \vec{V}_{F2}$), while the azimuthal angle φ is measured between the separation axis $\vec{V}_{PLF} - \vec{V}_{TLF}$ and the projection of the $\vec{V}_{F1} - \vec{V}_{F2}$ vector onto the reaction plane (see Fig. 6). Thus the angle ϑ , ranging from 0° to 180° , determines the out-of-plane angle of the PLF breakup axis. (In this convention the in-plane breakup corresponds to $\vartheta = 90^\circ$.) The azimuthal

angle takes a value $\varphi = 0^\circ$ when the projection of the fission axis onto the reaction plane coincides with the separation axis. The angle φ takes positive values when the projection of the fission axis turns toward the beam direction and becomes negative when it turns to the opposite direction (see Fig. 6). To complete the above definitions, the fragments F1 and F2 are numbered according to their velocity vectors \vec{V}_{F1} and \vec{V}_{F2} projected onto the PLF + TLF separation axis: F1 has a larger value of this projection than F2.

Having defined the previous quantities, we can now examine the breakup of PLF in more detail.

A. Angular distributions of PLF breakup fragments

The out-of-plane distribution of fragments from the PLF decay is shown in Fig. 7. The plot displays the fragments' distribution as a function of an angle ϑ between the PLF breakup axis and the vector normal to the reaction plane. The distribution is peaked at the reaction plane ($\vartheta = 90^\circ$), with a width (at half maximum) of about $\pm 20^\circ$. Thus Fig. 7 demonstrates that the observed ternary reactions are strongly focused in the reaction plane.

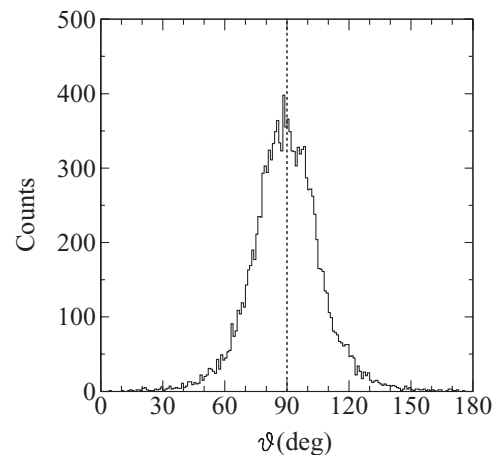


FIG. 7. Out-of-plane distribution of fragments from the PLF \rightarrow F1 + F2 breakup.

Crucial information on the mechanism of the studied ternary processes comes from examining features of the PLF breakup in its rest frame in the reaction plane. In Fig. 8 we show the angular distribution of the yield of fragments F1 and F2 and also of their average masses and relative velocities. All these observables are displayed as a function

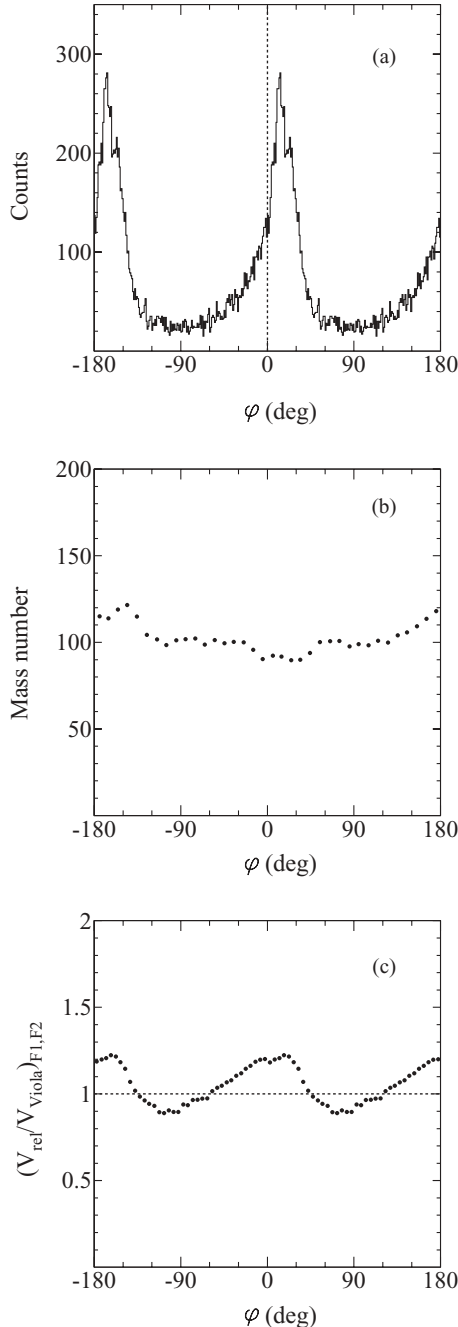


FIG. 8. Characteristics of the PLF \rightarrow F1 + F2 breakup in the rest frame of PLF as a function of the in-plane angle φ : (a) Distribution of fragments F1 and complementary fragments F2 projected onto the reaction plane, (b) distribution of the average mass number of fragments F1 and F2, (c) distribution of the average value of the relative velocity V_{rel} of fragments F1 and F2 in units of the “Viola velocity” V_{Viola} .

of the azimuthal in-plane angle φ defined earlier. As it is seen from Fig. 8(a), the in-plane angular distribution of fragments F1 is sharply peaked at an angle $\varphi \approx +15^\circ$, while the complementary fragments F2 are peaked at $\varphi \approx -165^\circ$. This angular distribution quantitatively demonstrates the effect of the almost exact alignment of all three fragments, F1, F2, and TLF, shown previously in the scatterplot in Fig. 5(a). The strong anisotropy of the in-plane angular distribution of fragments F1 and F2 proves that the PLF breaks up in a violent process, very different from the statistical fission of an equilibrated PLF.

Figure 8(b) shows the in-plane angular dependence of the average mass of fragments F1 and complementary fragments F2. In addition to the result displayed in Fig. 4, where mass-number distributions of fragments F1 and F2, integrated over all possible breakup angles, are presented, Fig. 8(b) shows how the average mass of the fragment F1 and complementary fragment F2 changes with the breakup angle φ .

Some essential information that may shed light on the physics of the PLF breakup is contained in Fig. 8(c), which shows the dependence of the relative velocity of fragments F1 and F2 on the in-plane PLF breakup angle φ . As explained in Sec. IV, the relative velocity V_{rel} is expressed in units of the “Viola velocity” V_{Viola} , corresponding to the kinetic energy of fission fragments of a fully equilibrated compound nucleus. One can see from Fig. 8(c) that the relative motion of fragments F1 and F2 is completely damped when the PLF breaks up perpendicularly to the PLF-TLF separation axis, while a distinct effect of incomplete equilibration is seen in the direction along the PLF-TLF separation axis when all three fragments, F1, F2, and TLF, are approximately aligned. By examining the angular distribution of the relative velocity more closely one can observe that the incomplete damping of the relative motion of the F1 + F2 subsystem is exactly correlated with the angular distribution of these fragments in Fig. 8(a). Evidently the generation of a kind of expansion mode (or a velocity gradient) directed along the PLF-TLF separation axis appears to be a necessary factor in the observed phenomenon of aligned ternary reactions.

For comparison, we show in Fig. 9 the angular distribution of the QMD theoretical events plotted together with the respective values of the relative velocity of fragments F1 and F2. As was seen already from Fig. 5(b), the theoretical events have practically isotropic distribution (a small modulation of the distribution is due to the detection efficiency filter applied to the theoretical events). The isotropy of the theoretical angular distribution is correlated with complete isotropy of the relative velocity. Therefore, it seems that even if the previously mentioned expansion mode were present in the theoretical events the relative motion of the F1 + F2 subsystem was later completely equilibrated.

B. Time scale of PLF breakup

A nearly collinear emission of all fragments in the observed ternary reactions [see Figs. 5(a) and 8(a)] demonstrates that these reactions must go very fast. In the following we attempt to quantitatively estimate the time scale of this process by making use of a small, but systematic effect of the deflection of the PLF

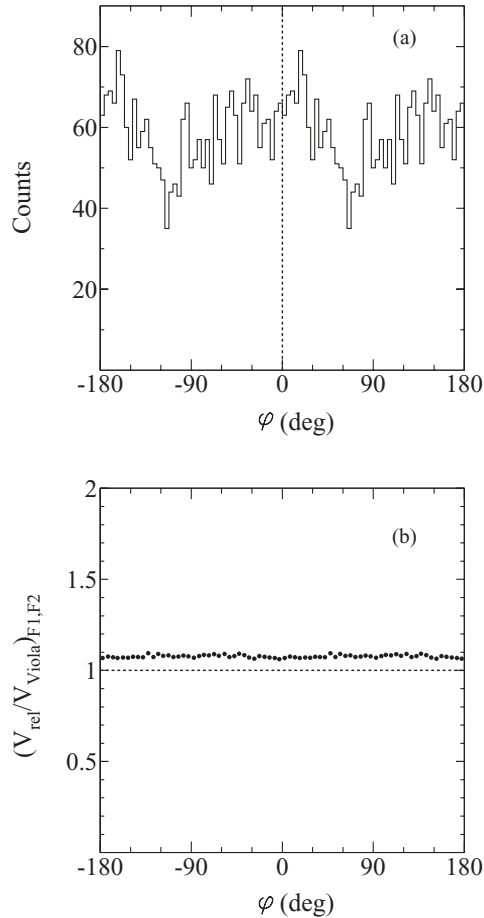


FIG. 9. (a) Angular distribution of fragments F1 and F2 in the theoretical sample of events generated with the QMD code [19] together with (b) angular distribution of the average relative velocity $(V_{\text{rel}}/V_{\text{Viola}})_{\text{F1,F2}}$, calculated the same way as for the experimental events in Fig. 8.

breakup axis from the direction of the PLF + TLF separation. This effect was used for the same purpose by Casini *et al.* [24].

We assume a two-step scenario of Eq. (4): In the first stage, the projectile and target nuclei undergo a strongly damped (deep-inelastic) collision in which a large amount of kinetic energy E_{TKEL} is dissipated and at the same time a considerable part of angular momentum of relative motion is transferred to rotational degrees of freedom. Consequently, during the reseparation stage, the system rotates and simultaneously stretches out until the PLF and TLF get separated from each other. In the second stage, both PLF and TLF continue to rotate and stretch and finally either one or both of them breakup (depending on the amount of deposited excitation energy, transferred angular momentum, and the kinetic energy associated with the stretching process). If the PLF were splitting immediately after the separation of PLF from TLF (i.e., at $\Delta t = 0$), we will observe fragments F1 exactly at the direction of the PLF-TLF separation axis at $\varphi = 0^\circ$. The observed deflection from this direction by an angle $\Delta\varphi$ is due to the rotation of the PLF during the time interval Δt elapsing from the separation of PLF from TLF to the separation of

fragments F1 and F2, for the process of Eq. (4)

$$\Delta t = \Delta\varphi \mathcal{J} / J, \quad (10)$$

where \mathcal{J} is the moment of inertia and J the intrinsic spin of the rotating PLF (transferred from the angular momentum of relative motion during the deep-inelastic collision). To estimate a value of the spin of PLF we used the nucleus-nucleus dynamics code HICOL of Feldmeier [25]. This classical model based on one-body dissipation dynamics well predicts the average losses of kinetic energy and the associated transfer of angular momentum as a function of the impact parameter. According to HICOL, to generate the inelasticity of the reaction $E_{\text{TKEL}} \approx 450$ MeV, corresponding to the location of the maximum of the observed spectrum of kinetic energy at $E_{\text{kin}}(\text{PLF} + \text{TLF}) \approx 1000$ MeV (see Fig. 3), it is necessary that the $^{197}\text{Au} + ^{197}\text{Au}$ system collides semiperipherally having an angular momentum $L \approx 0.68 L_{\text{max}}$ where L_{max} is the maximum value of angular momentum corresponding to the grazing collision, $L_{\text{max}} = 1160 \hbar$. For such a trajectory the transfer of angular momentum to PLF is $J \approx 75 \hbar$. The same HICOL calculation provides information on the second quantity in Eq. (10), the moment of inertia \mathcal{J} of the rotating PLF. The model predicts that, at the point of separation from TLF, the PLF has a shape (sphere plus a conic appendage) typical for scission configuration, with a value of $\mathcal{J} \approx 4500$ amu fm². Assuming this value of the moment of inertia we obtain for $J = 75 \hbar$ the time Δt of about 70–80 fm/c.

Note that by taking the initial value of the PLF moment of inertia we may somewhat underestimate Δt because \mathcal{J} increases on the way to the breakup of PLF. However, as the major part of the deflection angle $\Delta\varphi$ is due to the stage of the fastest rotation, in our estimate of Δt we used the initial value of \mathcal{J} .

As stated earlier, Δt is the time interval elapsing from the scission of the total system into PLF + TLF to the scission of PLF into fragments F1 and F2. The time $\Delta t = 70\text{--}80$ fm/c indeed is very short, comparable with the separation time of the PLF + TLF system. (During that time the distance between PLF and TLF increases only by about 8 fm.) We therefore conclude that the breakup of PLF in the observed ternary reactions occurs almost instantly, just after the primary deep-inelastic process.

VI. QUATERNARY REACTIONS

As seen from Fig. 1, only binary deep-inelastic reactions, ternary reactions, and quaternary reactions significantly contribute to the balance of possible partitions of the heavy $^{197}\text{Au} + ^{197}\text{Au}$ system. The contribution of the latter reaction mode is the smallest of these three, but in fact, it is considerably higher than it appears from Fig. 1 because, as will be shown later, the efficiency of detecting complete quaternary events was strongly suppressed in the experiment due to kinematical conditions. In the following we give the results of an analysis of the quaternary reactions, which represent a natural extension of the mechanism of ternary partitions: In the quaternary reactions both PLF and TLF undergo a similar process of fast dynamical breakup.

The selection of the quaternary events was done under the same conditions imposed on the mass and momentum balance as in the case of ternary events [see Eqs. (1)–(3), which should be modified now for a number of fragments $i = 4$]. Following the logic of the analysis of ternary events, also in the case of the quaternary reactions the four fragments were arranged according to their longitudinal velocities

$$V_{\text{long}}(F1) > V_{\text{long}}(F2) > V_{\text{long}}(F3) > V_{\text{long}}(F4), \quad (11)$$

and further analysis was made assuming a binary process in the primary stage



followed by secondary decay processes



It was assumed here that the two fastest fragments, F1 and F2, originate from the breakup of PLF while the two slowest fragments, F3 and F4, are products of the breakup of TLF. (Although the differentiation of the longitudinal velocities of fragments F1, F2, F3, and F4 was not so unambiguous as in the case of ternary reactions, the adopted scheme allowed us to reach important conclusions regarding the mechanism of the observed quaternary breakup reactions.)

Following the assumptions formulated earlier, the PLF velocity vector \vec{V}_{PLF} was reconstructed from the velocity vectors of the two fastest fragments, F1 and F2, while the TLF velocity vector \vec{V}_{TLF} was reconstructed from the velocity vectors of the two slowest fragments, F3 and F4. Similarly, as in the case of ternary reactions, the vector $\vec{V}_{\text{PLF}} - \vec{V}_{\text{TLF}}$ defines the separation axis and this axis together with the beam direction determine the reaction plane.

In Fig. 10(a) we present the quaternary events the same way as the ternary events are presented in Fig. 5(a). The range of the mass numbers of fragments F1 and F2 from the PLF decay in the ternary reactions [Eqs. (8) and (9)] is now extended also for the decay of TLF into F3 and F4

$$60 \leq A_{F3} < 150, \quad (14)$$

$$60 \leq A_{F4} < 150. \quad (15)$$

This choice of the range of mass numbers of fragments F1, F2, F3, and F4 (corresponding to the partition of the $^{197}\text{Au} + ^{197}\text{Au}$ system into four fragments of nearly equal size) encloses the most probable quaternary partitions observed in the experiment. Similarly as for ternary reactions, nearly coplanar ($\pm 20^\circ$) quaternary events are displayed in Fig. 10(a) in a common reaction plane and the sign of the transversal velocity of TLF (in the reaction plane) is assumed to be always negative.

Figure 10(a) demonstrates an amazing phenomenon of nearly collinear emission of all four fragments. One can roughly estimate the location in the velocity space of PLF and TLF prior to their breakup: $V_{\text{long}} \approx 4.2 \text{ cm/ns}$, $V_{\text{trans}} \approx 1.0 \text{ cm/ns}$ for PLF and $V_{\text{long}} \approx 1.0 \text{ cm/ns}$, $V_{\text{trans}} \approx -0.6 \text{ cm/ns}$ for TLF. These two locations determine the PLF + TLF separation axis indicated in Figs. 10(a), 10(b), and 10(c) by dashed lines. One can see from Fig. 10(a) that the observed four fragments indeed reparate almost collinearly along this direction. However, an effect of the rotation by a small angle,

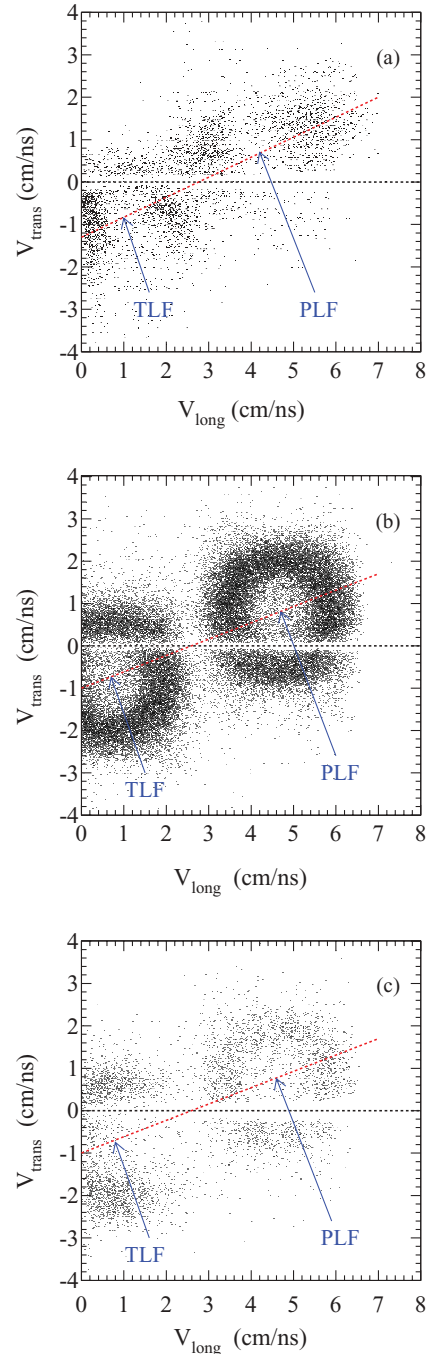


FIG. 10. (Color online) (a) In-plane velocity distribution of fragments from quaternary partitioning of the $^{197}\text{Au} + ^{197}\text{Au}$ system and (b) the same distribution generated with the QMD code [19]. The theoretical events filtered with the CHIMERA detector filter are shown in panel (c). Points represent velocities of fragments F1, F2, F3, and F4 in each quaternary event, plotted in the laboratory reference frame as a function of the longitudinal and transversal components. Positions of primary TLF and PLF are indicated by arrows. The dashed lines show the TLF-PLF separation axis. See text.

similar to the rotation of PLF in the case of the ternary events, is seen for both PLF and TLF. [See a more detailed, quantitative analysis of this effect in Figs. 11(a) and 11(b).]

In Figs. 10(b) and 10(c), we compare the observed pattern of the velocity distribution with that simulated with the QMD model [19]. Figure 10(b) shows the theoretical distribution unaffected by the detection efficiency, while Fig. 10(c) shows this distribution after applying the filter [20] of the CHIMERA detector. The theoretical events in Fig. 10(b) and 10(c) are selected for the same gates on fragments' mass numbers [Eqs. (8), (9), (14), and (15)] and for the same range of the out-of-plane angles of the PLF and TLF breakup ($\pm 20^\circ$) as in the analysis of the experimental data. It is seen from Fig. 10(b) that the QMD model correctly reproduces the kinetic energies of PLF and TLF in the primary stage of the deep inelastic collision (i.e., before the breakup of both these primary fragments). Also reproduced correctly is the resulting direction of the PLF + TLF separation axis. According to the QMD simulation, both PLF and TLF are predicted to breakup in these collisions, but in contrast to the experiment, the QMD model predicts almost isotropic angular distributions of fragment pairs F1 + F2 and F3 + F4 (in the rest frames of the PLF and TLF, respectively). By comparing the experimental and theoretical distributions of ternary and quaternary reactions (Figs. 5 and 10, respectively), one can see that the breakup of TLF and PLF in quaternary events looks the same as the breakup of PLF in ternary events. Evidently both classes of events originate from the same type of a deep-inelastic process that results in breaking up of either one or both primary fragments (PLF and TLF).

Analysis of quaternary events revealed that this group of events suffered particularly low detection efficiency despite the nearly complete geometrical coverage of the CHIMERA array. The reason for this is that, in the studied reaction at 15 MeV/nucleon, the backward directed TLF breakup fragments (F4) have very low laboratory kinetic energies and are stopped in the target in a major part of the events. (Contrary to that, ternary events, in which TLF does not breakup, are not influenced by this particular detection efficiency problem.) The effect of very low efficiency, dependent on the direction of the emission of the F4 fragment, is seen at a glance from Fig. 10 by comparing the velocity distributions of theoretical quaternary events prior to and after applying the detection filter [20], see Figs. 10(b) and 10(c), respectively.

Similarly as in the analysis of ternary reactions, the in-plane angular distributions of F1 and F2 fragments from the breakup of PLF and F3 and F4 fragments from the breakup of TLF are shown in Figs. 11(a) and 11(b), respectively, as a function of the azimuthal angle φ , defined in Sec. V. For the breakup of TLF, the azimuthal angle φ is defined the same way as for the PLF breakup in case of ternary events. For both distributions in Figs. 11(a) and 11(b) the angle φ is measured with respect to the direction of the PLF + TLF separation axis ($\varphi = 0^\circ$).

As stated earlier, in the case of the quaternary events the effect of the detection efficiency is of high importance. The measured in-plane distributions of fragments [dashed histograms in Figs. 11(a) and 11(b)] are severely distorted. The efficiency correction determined as the ratio of theoretical events found in a given element of phase space with the detection filter applied and without it restores the correct shape of the angular distributions (solid line histograms).

It is amazing that the in-plane angular distributions of F1 + F2 and F3 + F4 pairs of fragments in quaternary

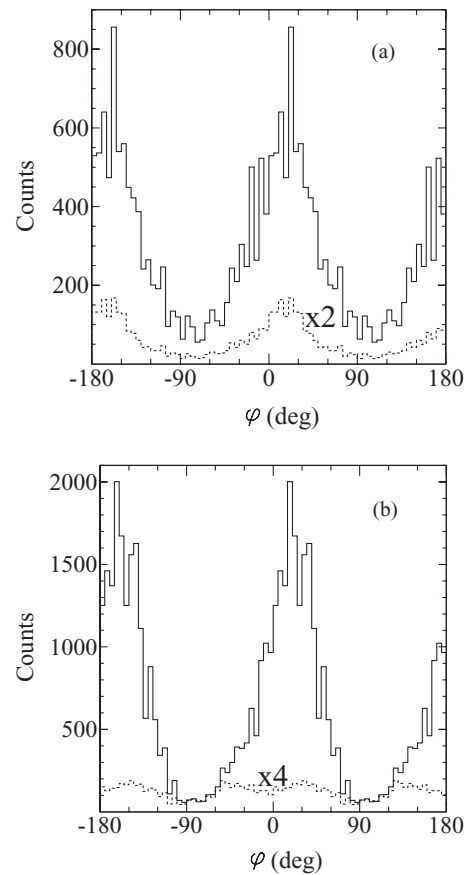


FIG. 11. In-plane angular distributions of fragments in quaternary reactions: (a) Distribution of fragments F1 and F2 from the PLF \rightarrow F1 + F2 breakup in the rest frame of PLF and (b) distribution of fragments F3 and F4 from the TLF \rightarrow F3 + F4 breakup in the rest frame of TLF. The measured dashed-line histograms were corrected, channel by channel, by a factor of the quaternary detection efficiency (solid-line histograms), see text.

events look very similar to the in-plane angular distribution of the F1 + F2 pair from the breakup of PLF in the case of ternary reactions, shown in Fig. 8(a). Similarly as in the ternary reactions, both primary reaction products PLF and TLF show the rotation by an angle, on the average, of about $\Delta\varphi = +15^\circ$ with respect to the PLF + TLF separation axis. This small deviation from the exactly collinear breakup of PLF and TLF can now be used to estimate the time scale of the quaternary reactions the same way as it was done for ternary reactions: The reconstructed kinetic energy spectrum for the quaternary events is peaked at $E_{\text{kin}}(\text{PLF} + \text{TLF}) \approx 650$ MeV, and thus, according to HICOL predictions [25], the corresponding localization of these quaternary reactions in the angular momentum space is at $L/L_{\text{max}} \approx 0.55$. This results in an average value of spin transferred to PLF or TLF to be $J \approx 64 \hbar$, while moments of inertia of these fragments (at scission configuration, calculated for PLF and TLF rotations around their individual centers of mass) equal to about $\mathcal{J} = 4500$ amu fm². Then, from Eq. (10) an estimate of the time elapsing from the PLF + TLF separation to the breakup of both PLF and TLF is obtained $\Delta t = 80\text{--}100$ fm/c (cf. the discussion on the time scale of ternary reactions in Sec. V).

VII. SUMMARY AND CONCLUSION

Our analysis shows that, in collisions of very heavy nucleus-nucleus systems such as $^{197}\text{Au} + ^{197}\text{Au}$ at energies of about 15 MeV/nucleon, we observe a new, very interesting reaction mechanism of violent reseparation of the interacting system into three or four massive fragments. The most likely scenario of these reactions is that a deep-inelastic binary process takes place in the first stage of the reaction that leads to the formation of two primary reaction products: PLF and TLF. Then either one of them (PLF in the case of the analyzed ternary events) or both (in the case of quaternary events) undergo a very fast breakup into two fragments of comparable size. The deep-inelastic scattering processes that lead to the observed ternary and quaternary reactions occur in deeply semiperipheral collisions: on average, at $L/L_{\text{max}} \approx 0.68$ and 0.55, respectively, where L_{max} is the maximum angular momentum corresponding to the most peripheral collisions. This localization of the ternary and quaternary reactions in L space was deduced from the peak positions of the reconstructed PLF + TLF energy spectra: $E_{\text{TKEL}} \approx 400$ and 800 MeV, respectively. Evidently, the ternary and quaternary reactions dominate the reaction cross section at those close collisions (at small L values) because the only really competing process, the binary reseparation, is strongly weakened at these small impact parameters.

The fact that the ternary and quaternary breakup reactions can occur only at relatively small impact parameters probably explains why they were not observed so clearly in collisions of lighter systems ($^{84}\text{Kr} + ^{166}\text{Er}$ and $^{129}\text{Xe} + ^{122}\text{Sn}$ [5] and $^{100}\text{Mo} + ^{100}\text{Mo}$ and $^{120}\text{Sn} + ^{120}\text{Sn}$ [6]) because, for those systems, such small impact parameters must preferentially lead to fusion. Consequently, a clear signature of fast, collinear breakup was observed in Ref. [6] only for very *asymmetric* partitions of PLF, probably occurring at larger impact parameters and originating from *neck fragmentation* processes, which are quite different in nature from the nearly symmetric PLF and/or TLF breakup reactions observed in the present work.

The most striking feature of the ternary and quaternary reactions observed in the studied $^{197}\text{Au} + ^{197}\text{Au}$ collisions is their nearly exact alignment along the axis of reseparation of PLF + TLF system in the first (binary) stage of the reaction. This fact immediately points at a very short time scale of the whole process of reseparation of the colliding system. Detailed analysis of angular correlations of fragments has led to an estimate of the time elapsing from the scission of the binary PLF + TLF system to the scission of PLF to be in the case of ternary reactions $\Delta t = 70\text{--}80$ fm/c or in the case of quaternary reactions $\Delta t = 80\text{--}100$ fm/c (the time elapsing from the scission of the PLF + TLF system to the scission of both PLF and TLF).

The observed ternary and quaternary partitioning processes were simulated theoretically with the microscopic QMD code of Łukasik [19]. It is very instructive that this model does predict the ternary and quaternary partitioning of the heavy $^{197}\text{Au} + ^{197}\text{Au}$ system at sufficiently small impact parameters. However, the characteristic collinear emission pattern is not explained by the QMD model.

Our analysis shows that the very fast (collinear) breakup is associated with the incomplete energy dissipation in the relative motion of fragments. This may suggest that an important improvement of the theoretical description requires an essential modification of the nucleon-nucleon interaction term. This issue leads to the long standing question of the nature of dissipative phenomena in the transitional region at low energies. Thus the spectacular phenomenon of very fast ternary and quaternary breakup appears to be crucial for the understanding of the dynamics of moderately heated nuclear matter. It will also be very important if other transport theories, for example, the stochastic BNV model [11] and the CoMD-II model [12]—very successful in the description of the neck fragmentation processes at intermediate energies—can be verified at lower energies on this crucial phenomenon of fast ternary and quaternary breakup.

-
- [1] A. Gobbi and W. Nörenberg, in *Heavy Ion Collisions*, edited by R. Bock (North-Holland, Amsterdam, 1980) Vol. 2, pp. 127–274.
 - [2] N. Cârjan, A. J. Sierk, and J. R. Nix, *Nucl. Phys.* **A452**, 381 (1986).
 - [3] R. L. Fleischer, P. B. Price, R. M. Walker, and E. L. Hubbard, *Phys. Rev.* **143**, 943 (1966).
 - [4] H. J. Becker, P. Vater, R. Brandt, A. H. Boos, and H. Diehl, *Phys. Lett.* **B50**, 445 (1974).
 - [5] P. Glässel, D. v. Harrach, H. J. Specht, and L. Grodzins, *Z. Phys.* **A 310**, 189 (1983).
 - [6] A. A. Stefanini *et al.*, *Z. Phys.* **A 351**, 167 (1995).
 - [7] R. J. Charity *et al.*, *Z. Phys.* **A 341**, 53 (1991).
 - [8] I. Skwira-Chalot *et al.*, *Phys. Rev. Lett.* **101**, 262701 (2008).
 - [9] E. De Filippo *et al.*, *Phys. Rev. C* **71**, 044602 (2005).
 - [10] E. De Filippo *et al.*, *Phys. Rev. C* **71**, 064604 (2005).
 - [11] V. Baran, M. Colonna, and M. Di Toro, *Nucl. Phys.* **A730**, 329 (2004).
 - [12] M. Papa *et al.*, *Phys. Rev. C* **75**, 054616 (2007).
 - [13] A. Pagano *et al.*, *Nucl. Phys.* **A734**, 504 (2004).
 - [14] P. Russotto, Ph.D. thesis, University of Catania, 2006.
 - [15] V. E. Viola, K. Kwiatkowski, and M. Walker, *Phys. Rev. C* **31**, 1550 (1985).
 - [16] D. J. Hinde, J. R. Leigh, J. J. M. Bokhorst, J. O. Newton, R. L. Walsh, and J. E. Boldeman, *Nucl. Phys.* **A472**, 318 (1987).
 - [17] J. Wilczynski and K. Siwek-Wilczynska, *Phys. Rev. C* **41**, R1917 (1990).
 - [18] J. Töke, R. Planeta, W. U. Schröder, and J. R. Huizenga, *Phys. Rev. C* **44**, 390 (1991).
 - [19] J. Łukasik, computer code QMD-CHIMERA, (unpublished); J. Łukasik and Z. Majka, *Acta Phys. Pol. B* **24**, 1959 (1993).
 - [20] W. Gawlikowicz, Jagiellonian University, Cracow, Report No. ZFGM-03-02, 2003.
 - [21] E. Plagnol *et al.*, *Phys. Rev. C* **61**, 014606 (1999).
 - [22] R. J. Charity *et al.*, *Nucl. Phys.* **A483**, 371 (1988).
 - [23] W. Gawlikowicz, *Acta Phys. Pol. B* **28**, 1687 (1997).
 - [24] G. Casini *et al.*, *Phys. Rev. Lett.* **71**, 2567 (1993).
 - [25] H. Feldmeier, *Rep. Prog. Phys.* **50**, 915 (1987) <http://theory.gsi.de/~feldm/>.